CrossMark

Comparison Between Tsunami Signals Generated by Different Source Models and the Observed Data of the Illapel 2015 Earthquake

Ignacia Calisto,[1] Matthew Miller,[1] and Iván Constanzo[1]

Abstract—A major interplate earthquake occurred on September 16th, 2015, near Illapel, central Chile. This event generated a tsunami of moderate height, however, one which caused significant near field damage. In this study, we model the tsunami produced by some rapid and preliminary fault models with the potential to be calculated within tens of minutes of the event origin time. We simulate tsunami signals from two different heterogeneous slip models, a homogeneous source based on parameters from the global CMT Project, and furthermore we used plate coupling data from GPS observations to construct a heterogeneous fault based on a priori knowledge of the subduction zone. We compare the simulated signals with the observed tsunami at tide gauges located along the Chilean coast and at offshore DART buoys. For this event, concerning rapid response, the homogeneous source and coupling model represent the tsunami at least as well as the heterogeneous sources. We suggest that the initial heterogeneous fault models could be better constrained with continuous GPS measurements in the rupture area, and additionally DART records directly in front of the rupture area, to improve the tsunami simulation based on quickly calculated models for near coastal areas. Additionally, in terms of tsunami modeling, the source estimated from prior plate coupling information in this case is representative of the event that later occurs; placing further importance on the need to monitor subduction zones with GPS.

Key words: Tsunami signal, slip model distribution, earthquake rupture.

1. Introduction

Central Chile has suffered numerous large earthquakes which have generated devastating tsunamis. These tectonic events are related to the subduction of the Nazca plate beneath the South American continent at a speed of ~ 68 mm/year (Angermann and Klotz 1999; Vigny *et al.* 2009). In consequence, events with a considerable magnitude have occurred

periodically in the study area; the latest of these being the Illapel earthquake (Mw $\simeq 8.2$) occurring on the 16th of September, 2015, generating a moderate tsunami which reached a maximum recorded height of 4.5 m in Coquimbo.

The rupture area is located approximately between the latitudes of 30° and 32.5°S, and cities of considerable population were affected by the earthquake and tsunami. Tsunamigenic earthquakes have been registered in this area since 1730, the events of 1880 and 1943 being the two most recent (Lomnitz 1971; Compte and Pardo 1991). The subduction geometry shows unusual behavior at these latitudes, since the slab becomes nearly flat at around 100 km depth (Tassara *et al.* 2006; Pardo *et al.* 2012) and arc volcanism is cut off (Stern 2004). The rupture area of the Illapel earthquake, and its predecessors, is delimited to the north by the Challenger fracture zone and to the south by the Juan Fernandez ridge (Sparkes *et al.* 2010).

To quickly estimate tsunami height and first wave arrival time, homogeneous fault models can be used. However, to have a better understanding of the tsunami source, more realistic models can be simulated (Calisto *et al.* 2015). Heterogeneous models are based on a wide range of observations that include seismological, GPS, and even tsunami measurements. The main problem, regarding tsunami hazard mitigation, is the time required to generate these heterogeneous models; those based only on seismological data are currently the quickest available.

A tsunami brings information about its source and propagation to coastal, and deep water, tide and pressure gauges. In this study, we compare the observed tsunami generated by the 2015 Illapel event to simulated signals, using different source models, at

[1] Geophysics Department, University of Concepcion, Concepción, Chile. E-mail: icalisto@dgeo.udec.cl

six tide gauge locations along the Chilean coast and three offshore DART buoys.

2. Tsunami Modeling

The tsunami numerical simulation is computed using the software COrnell Multi-grid Coupled Tsunami Model (COMCOT), version 1.7 (Wang 2009), which adopts staggered leap-frog finite differences to solve shallow water equations in their linear and non-linear form (Liu et al. 1998). The linear approximation is used when the wavelength is much larger than the sea depth; the non-linear approximation is required as the wave approaches the coast and the bathymetry changes sharply. COMCOT v1.7 assumes that the uplift motion is much faster than the wave propagation, so the initial vertical water displacement is approximated by the sea floor displacement, calculated here using the improved elastic finite fault plane theory of Okada (1985). Furthermore, in this study we assume that all deformation occurs simultaneously.

COMCOT v1.7 uses a nested and equally spaced grid system, which reduces computational costs while allowing fine bathymetry grids near the coastline. We use four grid levels at six coastal locations; the nearest around 140 km from the epicenter and the farthest 1400 km away. At three offshore DART locations two grid levels are used. We simulate 3.5 h of tsunami propagation with a 5 s time step. We used a bottom friction coefficient of 0.025, representative of a 2 cm diameter coarse sand and widely used in tsunami simulation (Masamura et al. 2000).

3. Grid Generation

The nine locations chosen for this study are named in Table 1 and displayed in Fig. 1. Tide gauge data are available for the coastal and offshore locations and high resolution bathymetry is used for the coastal locations. The Generic Mapping Toolkit (Wessel et al. 2013) and ArcGis 9.3 are used to construct the four grid levels, generating in total 23 grids. There are two first level grids, with a resolution of 2.16 arc minutes, one is common for all coastal locations and covers the area from Arica to Talcahuano, and the other one is common for all the DART locations. Then, for the nine individual locations, second grids, with a 0.54 arc minutes resolution, were built. Third and fourth grid levels are generated with respective resolutions of 0.108 and 0.018 arc min for the coastal areas.

The level 1 grid resamples ETOPO1 (Amante and Eakins 2009) while the level 2 grid resamples NASA's SRTM30 plus data (Becker et al. 2009). The higher resolution bathymetry, used for the third and fourth level grids, is provided by the Chilean Navy Hydrographic and Oceanographic Service (Spanish acronym: SHOA) which has a maximum resolution of around 30 m (http://www.shoa.cl/tramites/tramite.php); this is coupled to the ASTER high resolution topography (http://asterweb.jpl.nasa.gov).

4. Tsunami Signals

4.1. Observed Data

The observed data are acquired from SHOA tide gauges situated close to the coastal cities of Arica, Iquique, Caldera, Coquimbo, Valparaiso and Talcahuano; and from NOAA's National Data Buoy Center (http://www.ndbc.noaa.gov/) for the offshore locations, which correspond to water column height from DART Buoys. For the coastal locations, the oceanic tide, simulated using a classical harmonic analysis, is subtracted to obtain the tsunami waveform. The DART data were filtered to remove the diurnal, semi-diurnal and lunar (M_3) tides. The resulting time series represents the tsunami signal, tidal signals with four or more cycles are not expected in deep ocean (Tolkova 2010). Table 1 summarizes the precise locations of the tide gauges and DART buoys.

4.2. Fault Models

Four different source models are used in this study, their surface deformations are shown in Fig. 2. The simplest model is a homogeneous rectangular fault, with parameters obtained from the Global Centroid Moment Tensor Project (http://www.globalcmt.org/) (Dziewonski et al. 1981; Ekström

Table 1

Summary of tide gauge and DART buoy locations

	Latitude	Longitude	Real depth (m)	Virtual depth (m)
Arica	18.48S	70.32W	4.43	4.76
Iquique	20.21S	70.15W	5.36	5.28
Caldera	27.10S	70.83W	4.59	3.77
Coquimbo	29.95S	71.33W	4.08	5.17
Valparaiso	33.03S	71.63W	4.58	11.63
Talcahuano	36.69S	73.11W	4.68	6.06
DART 32412	17.99S	86.33W	4387	4357
DART 32401	20.47S	73.43W	4797	4734
DART 32402	26.74S	73.98W	4070	4066

et al. 2012). This model has a moment magnitude of 8.2, a fault geometry with strike 5°, dip 22° and rake 106° at a centroid depth of 17.8 km and epicenter at 31.22°S, 72.27°W. We use the relations given by PAPAZACHOS *et al.* (2004), which relate the event magnitude to the length and width of the fault, and KANAMORI and ANDERSON (1975) to compute the slip, taking the rigidity, μ, to be 3×10^{10} Pa. The solutions give an area of 209×82 km^2 and average dislocation of 5.59 m. These values are consistent with the parameters calculated based on BLASER *et al.* (2010), STRASSER *et al.* (2010), KAMIGAICHI (2011) and MUROTANI *et al.* (2013). The resulting vertical surface deformation produced by this source is shown in Fig. 2d.

Two heterogeneous models based on seismological observations were used to simulate tsunami waveforms. The first one is the finite fault model obtained from the USGS event page (http://earthquake.usgs.gov/earthquakes/eventpage/us20003k7a). This solution is a preliminary finite fault model based on teleseismic waveform analysis. Figure 2a shows the surface deformation produced. On the other hand, the model of BENAVENTE *et al.* (2016) corresponds to a solution obtained using three component W-phase waveforms (KANAMORI 1993) acquired from the Federation of Digital Seismograph Networks (FDSN). The data selection and inversion procedures largely follow BENAVENTE and CUMMINS (2013). Additionally, the faulting surface in this solution is parametrized to follow the slab geometry provided by the SLAB1.0 model (HAYES *et al.* 2012). The surface deformation produced by this solution is shown in Fig. 2b.

We finally construct a heterogeneous model based on information collected prior to the 2015 earthquake: the plate locking within the area delimited by the last megathrust event in this area (1943), the subduction velocity, and the amount of time since the previous event. The interseismic coupling data of METOIS *et al.* (2014) used GPS data, collected between 2004 and 2012, to quantify the kinematic coupling on the subduction interface producing a plate locking distribution in the Atacama area. Assuming that the previous subduction event resets the stress accumulation in the system and that the locking degree has no temporal variation, the amount of slip that the slab should move during an earthquake is related to the degree of locking on the interface and to the amount of time during which the system is loading. It has previously been observed that plate locking patterns follow the slip distribution of large earthquakes (MORENO *et al.* 2010). We restrict the area of the source to the 1943 earthquake (BECK *et al.* 1998) and use this year to compute the amount of time for which the energy has accumulated, at a velocity provided by the plate motion code of DEMETS *et al.* (1994). The predicted heterogeneous slip distribution in this region is then the product of the plate locking degree, subduction velocity, and amount of time since last event. To obtain the rest of the fault parameters for each subfault we use the SLAB1.0 model (HAYES *et al.* 2012) for depth, strike and dip, and the pmotion code (DEMETS *et al.* 1994) for rake angle. The resulting surface deformation pattern is shown in Fig. 2c.
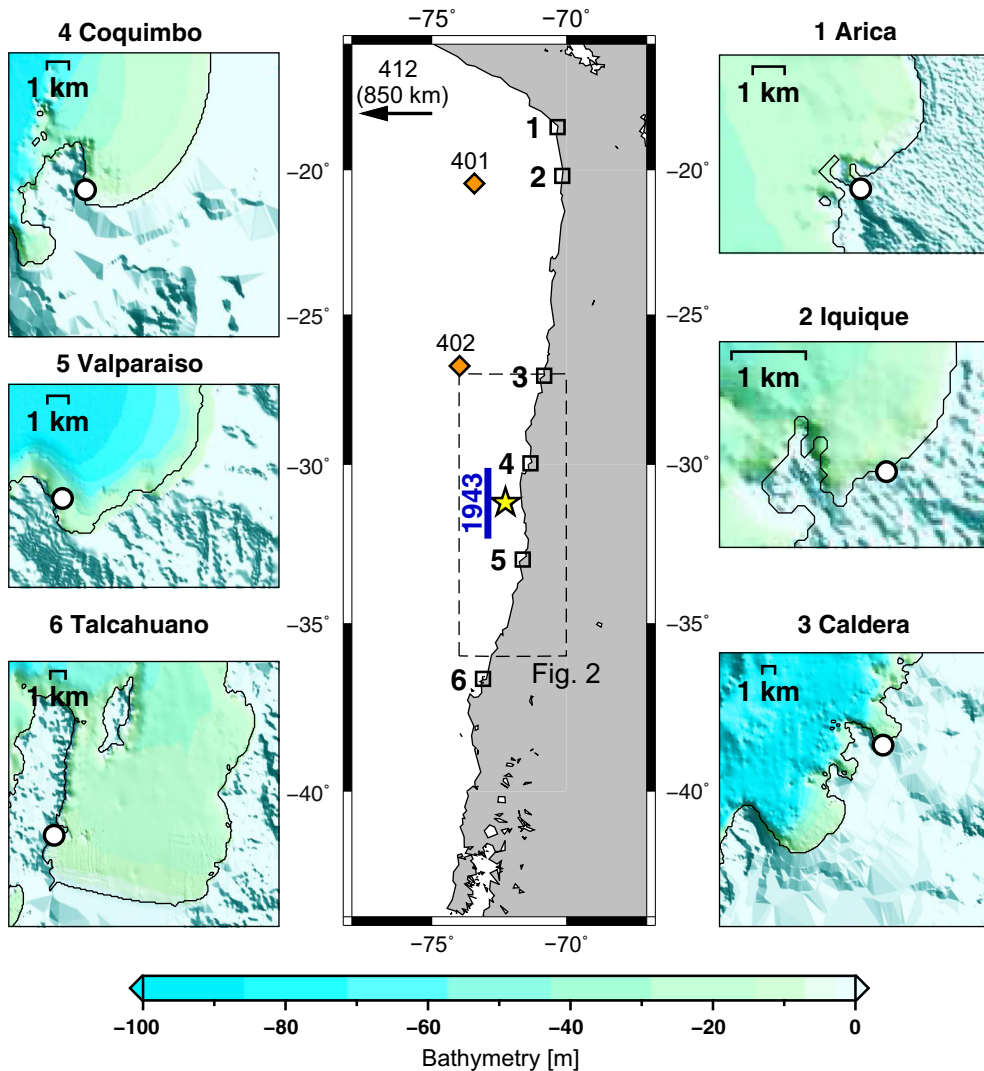
Figure 1

Central map: the study location in Chile, showing the limits of Fig. 2 (*dashed line*); 2015 epicenter from the global CMT solution (*yellow star*); 1943 event rupture limit, which activated again in 2015 (*blue line*); the positions of DART buoys 32401 and 32402 (*orange diamonds*), with the direction and distance to DART buoy 32412 off the map indicated by the *arrow*; and finally the six coastal locations used in this study (*numbered squares*). Side maps: the fourth level bathymetry grids used for the six coastal locations (correspondingly numbered and named) with the coastline estimation and precise location of the tide gauges (*white circles*)

5. Results

During the 3.5 h tsunami simulation the waves reach the six tide gauge locations along the coast and the three DART buoys. In the coastal areas, the farthest gauges are 1400 km north, and 650 km south, of the epicenter; the nearest, Coquimbo, is located 140 km to the north. The DART signals used are from buoys between 500 and 2000 km from the rupture area. The results of the observed tide gauge signals, compared to those generated by the different sources for coastal areas, are shown in Fig. 3. For the offshore locations this information is shown in Fig. 4.

In general, the four models can simulate the shape and arrival time of the tsunami. In the case of coastal tide gauges, the farthest stations show better fit, whereas for the offshore locations the main features of the DART records are well simulated. A
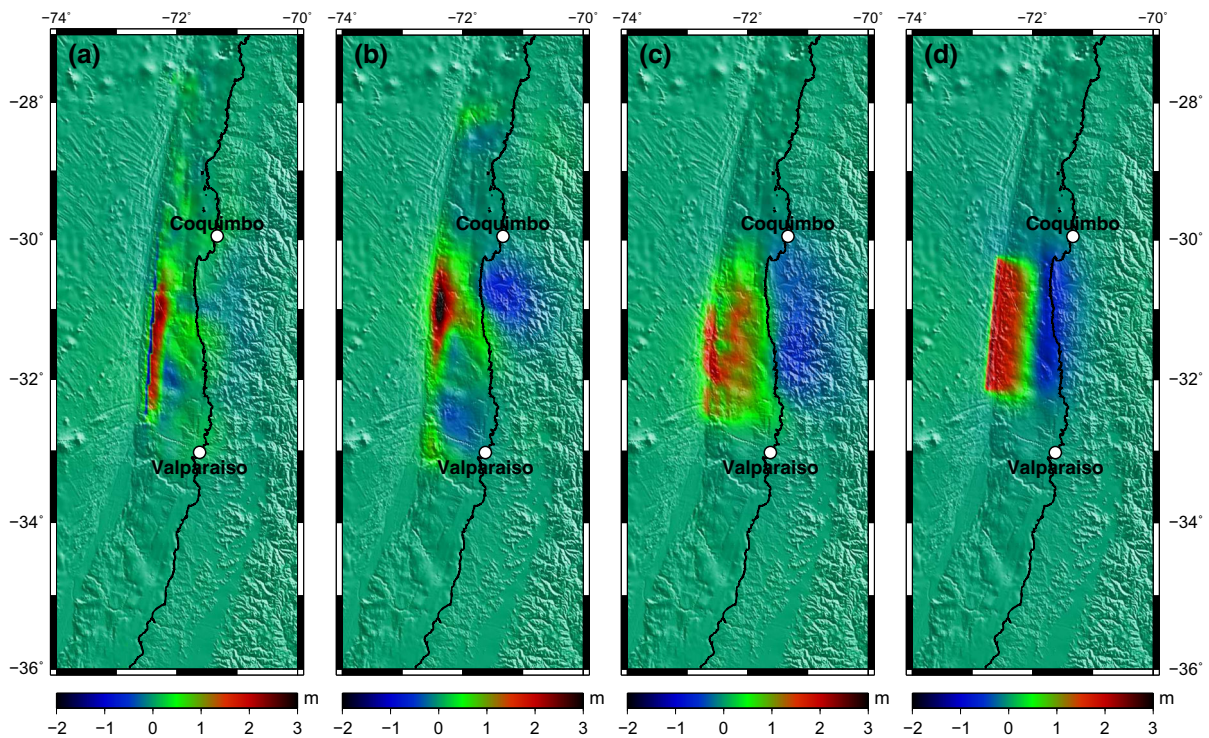
Figure 2
Initial deformation of the tsunami model using: **a** USGS preliminary model, **b** Benavente W-phase model, **c** Coupling distribution based on METOIS *et al.* (2014), and **d** Homogeneous fault model. The *white circles* are the nearest tide gauge locations to the epicenter and correspond to the boxes 4 and 5 of Fig. 1. The positions of the other tide gauges and DART buoys relative to the limits of this figure can also be seen in Fig. 1

measurable difference between the models is the wave amplitude, therefore we introduce a parameter which measures how well the amplitude of the first peak can be reproduced: the Spga parameter of AN-DERSON (2004), defined by

$$S(p_1, p_2) = 10 \exp\left\{ -\left[\frac{(p_1 - p_2)}{\min(p_1, p_2)} \right]^2 \right\}$$

where p_1 and p_2 are the amplitudes of the first peak of the observed and virtual tsunami signals. This is a function which decreases monotonically from the best fit value of 10. The results are displayed in Table 2.

Because we are investigating the source of the tsunami and how this influences its propagation, we concentrate mainly on the first wavelength, but also we extend the discussion to the extended wave train. For the coastal locations, the source contributes relatively more to the shape of the first wavelength, compared to the following waves. The first wavelength is less influenced by the physical consequences of the local geomorphology, such as shelf and bay resonance (YAMAZAKI and CHEUNG 2011; BELLOTTI *et al.* 2012). However, the following waves can be well modeled at the coastal locations if the tsunami source is accurately defined, for example see CALISTO *et al.* (2015) for results from a previous earthquake, and for the Illapel event the simulations from Aránguiz et al. (2016) and the Center for Tsunami Research (NOAA/PMEL) (http://nctr.pmel.noaa.gov/chile20150916/). For the case of the offshore locations, without the influence of the coast which amplifies the source errors forewards through time, we consider the entire simulation.

In Arica and Iquique, the gauges farthest north of the epicenter, the arrival time and shape of the first peak are well reproduced for all models; nevertheless, the amplitude is better estimated using the homogeneous and coupling-based models, as shown by their high Spga parameters. The USGS preliminary model significantly underestimates the wave height.
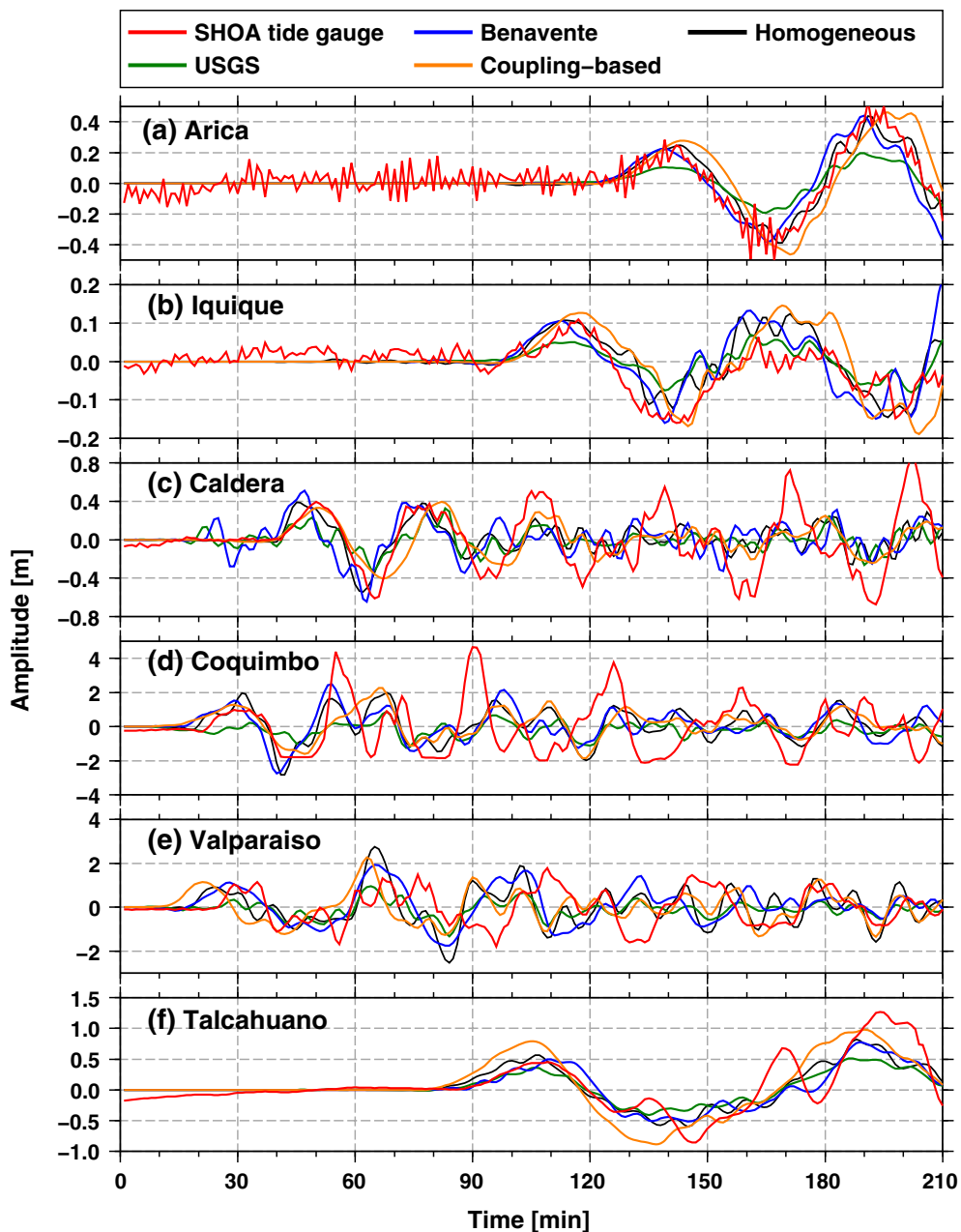
Figure 3
Comparison between the observed tsunami signal at SHOA tide gauges (*red line*) and simulated tsunami signal generated by different source models: USGS preliminary model (*green line*), Benavente W-phase model (*blue line*), Heterogeneous model based on interseismic coupling (*orange line*) and Homogeneous fault model (*black line*). Time is measured relative to the earthquake origin

Caldera is located 450 km north of the epicenter and the signals show good correlation for up to 120 min after the earthquake; beyond this, however, no model used in this study reproduces the observed waves. Again, the USGS preliminary model underestimates the

amplitude while the homogeneous, W-phase and coupling-based models all perform relatively accurate simulations for the first few wavelengths.

Coquimbo is the nearest location to the epicenter at which a tide gauge recorded the observed tsunami,
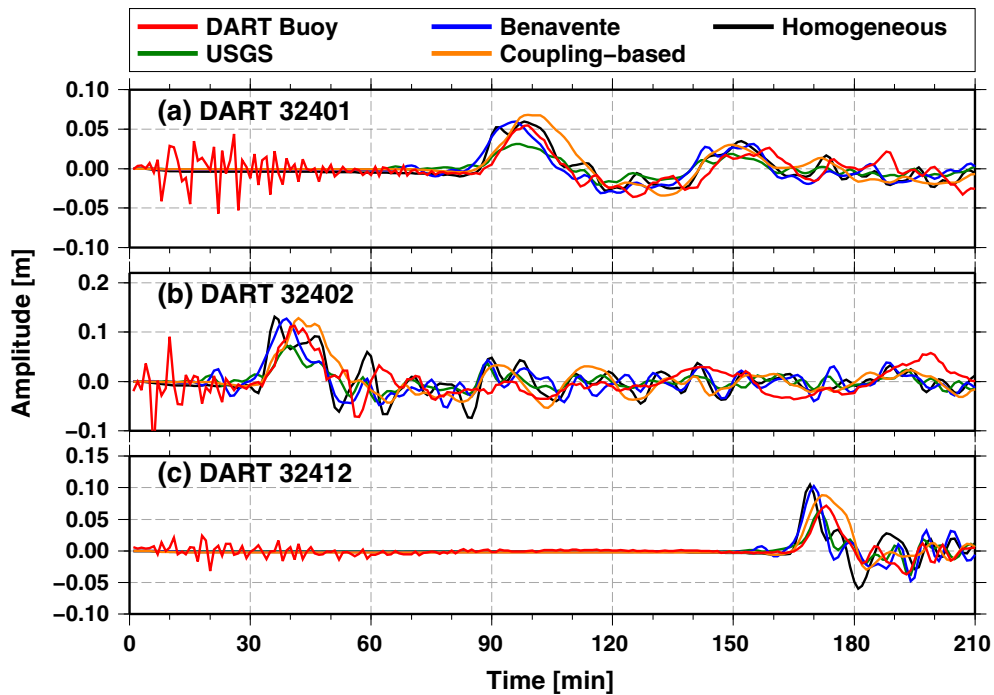
Figure 4
Comparison between the observed tsunami signal at DART buoys (*red line*) and simulated tsunami signal generated by different source models: USGS preliminary model (*green line*), Benavente W-phase model (*blue line*), Heterogeneous model based on interseismic coupling (*orange line*) and Homogeneous fault model (*black line*). Time is measured relative to the earthquake origin

situated just to the north of the rupture area. The first observed wave is again similar to that of the coupling-based model, the only one to have a high Spga parameter. No model used here can accurately reproduce the second and fourth waves which reach over 4 m in height. Concerning the first three waves only, the W-phase model of Benavente, which predicts the greatest uplift close to the trench in front of Coquimbo, produces the best fit.

In Valparaiso, situated close to the southern extent of the rupture area, the models do not reproduce the entire 210 min observation, although a high-frequency component on both the observed and modeled data complicates the visual interpretation. The shape and amplitude of the first peak is well fit for the homogeneous, coupling-based, and W-phase models. The Spga parameters confirm the goodness of fit for the first peak amplitude; however, it should be noted that they are time shifted. Furthermore, the coupling-based model overestimates the arrival time, the simulated tsunami appears 15 min early.

The southernmost location, Talcahuano, is 650 km south of the epicenter. The first wave is best represented by the homogeneous model while the two heterogeneous models derived from seismic data are very similar in form and slightly underestimate the observed amplitude, although still with good Spga values; finally the coupling-based model overestimates the amplitude and the arrival time of the first peak. The arrival time of the second wave, observed around 170 min after the event origin time, is not reproduced by any model.

The DART buoy 32401 is located 1200 km northwest of the earthquake epicenter and the virtual signals fit the general shape of the record for the length of the simulation. The coupling-based and homogeneous models fit the arrival time of the first wave better, whereas the amplitude is well reproduced by the W-phase and homogeneous models, as the Spga coefficient confirms.

The closest DART buoy, 32402, is located 500 km from the epicenter. The arrival time is better

Table 2

Spga parameter which measures the goodness of fit of the first peak

	USGS preliminary	Benavente	Coupling-based	Homogeneous
Arica	0.09	4.74	9.71	9.03
Iquique	2.08	8.15	9.93	10.00
Caldera	7.80	9.76	9.87	9.99
Coquimbo	5.25	3.48	9.46	3.46
Valparaiso	4.36	9.98	9.97	9.98
Talcahuano	9.27	9.32	6.16	9.39
DART 32412	9.83	8.42	9.52	7.58
DART 32401	5.81	9.89	9.41	9.95
DART 32402	8.26	9.77	9.71	8.21

obtained by the coupling-based model as well as the signal shape, although the amplitude is a little over-estimated. The homogeneous, W-phase and USGS models generate more subsequent waves than the coupling-based model, but none are capable of accurately matching the observation.

The DART buoy 32412 is the furthest tsunami signal, 2000 km distant from the epicenter. The arrival time for the first wave is well reached by the coupling-based and USGS models, and the Spga parameter confirms that those models also better fit the amplitude.

6. Discussion

The two heterogeneous source models which can rapidly be calculated for this earthquake, based on teleseismic waveform data, produce tsunami signals which generally represent the waves observed along the Chilean coastline. Additionally, the W-phase model of Benavente provides a good tsunami fit when compared to the preliminary USGS model which uses the more traditional seismic phases (P, SH and surface).

Somewhat surprisingly, among the three fault models based on earthquake data, it is the homogeneous finite fault that gives the best first wavelength fit for the tsunami signal. This can be explained by limitations on either the heterogeneous source models or the tsunami simulation and bathymetry used. However, a prior study of the 2014 Iquique earthquake (CALISTO et al. 2015) has demonstrated that it is possible to accurately model a near field tsunami in Chile using SHOA bathymetry, in which the

heterogeneous source models were inverted using coseismic GPS measurements along with teleseismic waveforms. It is worth noting that later peaks at the closest tide gauges are not well predicted by any model used in this study, suggesting a different, potentially more complicated fault mechanism than one which can be rapidly obtained from long-period teleseismic phases. A recent study (HICKS and RIET-BROCK 2015) has demonstrated that greater source detail can be found using higher frequency near field seismic data, information which is lost in the teleseismic waveforms. This suggests that a combination of real-time, near field, seismic and GPS stations, providing additional constraints for the slip inversions, could improve the correlation between quickly modeled and observed tsunami signals.

We next focus on the nearest tide gauge, Coquimbo, at which the amplitudes of the second and fourth waves are underestimated. The first peak, which is better reproduced, is the consequence of the sea floor uplift closest to the gauge. Beyond this distance range, we suggest that relatively small perturbations to the source mechanism have the potential to alter this waveform after the first peak, as any changes in wave directionality will be strongly affected by the bay geometry, especially as the northernmost rupture limit is around the same latitude as the bay. The W-phase model of Benavente, which gives the greatest vertical displacement in front of Coquimbo, is the closest to obtaining the observed wave amplitudes. If more data sources were available, further slight modification of this slip distribution in the northern part of the rupture area could significantly improve the model at this tide gauge.

The coupling-based model uses information gathered in the rupture area prior to 2015 to generate a heterogeneous source model. Therefore, the success of this model in matching the main features of the generated tsunami in 2015 is a notable result. However, this is not without complications: the overestimated arrival time, especially at Valparaiso, is due to the 2015 event having less slip in the southernmost part of the rupture area than the coupling predicts. This cannot currently be improved post-event, as the coupling-based model uses no parameters of this event in its definition, instead taking all of its information from the loading stage of the seismic cycle. The coupling model has limitations due to the distribution of the GPS stations, and also as the land-based GPS have less control over the offshore coupling values, meaning lower resolution near the subduction trench, the area which has the most influence over tsunami generation. In this study in particular, there is a lower density of GPS stations in the southern limit of the rupture area, see Fig. 3 of METOIS et al. (2014). More work is required in this topic to confirm the suitability of coupling maps to predict the characteristic features of future tsunamis.

To evaluate source models, the coastal tide gauge data have limitations: they are sited in sheltered locations and the complexity of the near shore bathymetry accentuates any small perturbations in the tsunami waveforms caused by source errors. In contrast, the DART records are free of harbor effects so provide more reliable information for source estimation. We suggest that the differences between the DART and simulated signals can be mainly attributed to source errors in the quickly derived slip models. Although the tsunami, in this case, arrives at the DART buoys after the seismic information used to construct the sources is available, DART data clearly can improve upon the initial seismic source estimates (TANG et al. 2016) and more accurately predict Pacific-wide propagation (see http://nctr.pmel.noaa.gov/chile20150916/ for more information).

7. Conclusions

For rapid response and tsunami mitigation after a seismic event, the rupture models predicted by the teleseismic waveforms produce usable initial tsunami estimates. The W-phase model is promising; this phase arrives before the S and surface waves, meaning it is theoretically possible to model the slip and produce an initial tsunami prediction as soon as the W-phase arrives, within 5 min at regional stations (YE et al. 2016) and around 20 min at seismic stations up to 5000 km distant (KANAMORI and RIVERA 2008; HAYES et al. 2009). While the tsunami estimated from these slip models is far from perfect, in this study they reproduce the amplitudes and arrival times of the tsunami arriving at coastal areas sufficiently well to aid tsunami warning and mitigation attempts. To further improve these models within the required timescale, a potential way could be through real-time GPS measurements in the vicinity of the rupture area. Previous studies (CALISTO et al. 2015) have shown success in simulating tsunamis from GPS-derived source models for other subduction earthquakes (SCHURR et al. 2014); however, the accuracy of such methods for tsunami source estimation is still not proven. An increased density of real-time GPS coverage along subduction zones would help future studies in this topic.

DART data would help to refine the quickly calculated, seismic-based slip models, and to model a source to enable more accurate simulation across the Pacific area. In this case, the closest DART buoy records the tsunami half an hour after the event origin time. However, with DART buoys directly in front of the rupture, it would be possible to use DART data quicker to constrain the predicted affects of the tsunami and its propagation along the near coastal areas. Chile is one of the World's most seismically active countries and currently only has two offshore DART buoys, both situated in the north. It would be helpful for future events to have more buoys operational in this corner of the Pacific.

In tsunami hazard analysis, potential sources used to generate inundation maps are often homogeneous models which do not necessarily produce the best fit to the eventual event (CALISTO et al. 2015). In this study, we show that a reasonable heterogeneous slip model can be predicted by an interseismic degree of locking. Figure 3 and Table 2 show that the coupling-based model generally performs well in shape, first peak amplitude and arrival time. GPS

observations and the generation of accurate, high resolution locking degree datasets for regions where subduction earthquakes periodically happen could be used to predict more realistic heterogeneous tsunami source models before the earthquakes happen. Tsunami inundation maps could be updated using this information to give the scenario arising from the most representative source in a particular region. However, more work is required at other subduction zones to confirm this hypothesis.

GPS stations are of great use for subduction zones, concerning tsunami hazard estimation, for two main reasons: not only could continuous GPS sites help to constrain preliminary fault slip models (and the simulated tsunami they generate), but also GPS data can generate the plate locking maps which could provide a representative tsunami source estimate prior to the event happening. The collection and transmission of both onshore and offshore data, real-time automation of slip models and tsunami estimates, and further understanding of subduction zone segmentation and earthquake cycles are ongoing challenges concerning accurately simulating and predicting future tsunamis, and the damage they will cause.

REFERENCES

AMANTE, C. and B. W. EAKINS (2009), *ETOPO1 1 Arc-Minute Global Relief Model: Procedures, Data Sources and Analysis.*

NOAA Technical Memorandum NESDIS NGDC-24. National Geophysical Data Center, NOAA. doi:10.7289/V5C8276M.

ANGERMANN, D. and J. KLOTZ (1999), *Space-geodetic estimation of the Nazca-South America Euler vector*, Earth planet. Sci. Lett., *171*, 329-334.

ANDERSON, J. (2004), *Quantitative measure of the goodness-of-fit of synthetic seismograms*, 13WCEE conference, paper No 243.

ARÁNGUIZ, R., G. GONZÁLEZ, J. GONZÁLEZ, P. A. CATALÁN, R. CIENFUEGOS, Y. YAGI, R. OKUWAKI, L. URRA, K. CONTRERAS, I. RIO and C. ROJAS (2016), *The 16 September 2015 Chile Tsunami from the Post-Tsunami Survey and Numerical Modeling Perspectives*, Pure and Appl. Geophys., *173(2)*, 333–348, doi:10.1007/s00024-015-1225-4.

BECK, S., S. BARRIENTOS, E. KAUSEL and M. REYES (1998), *Source characteristics of historic earthquakes along the central Chile subduction zone*, J. South Am. Earth Sci., *11:2*, 115-129.

BECKER, J. J., D. T. SANDWELL, W. H. F. SMITH, J. BRAUD, B. BINDER, J. DEPNER, D. FABRE, J. FACTOR, S. INGALLS, S.-H. KIM, R. LADNER, K. MARKS, S. NELSON, A. PHARAOH, R. TRIMMER, J. VON ROSENBERG, G. WALLACE and P. WEATHERALL (2009), *Global Bathymetry and Elevation Data at 30 Arc Seconds Resolution: SRTM30 PLUS*, Marine Geodesy, *32:4*, 355-371.

BELLOTTI, G., R. BRIGANTI and G. M. BELTRAMI (2012), *The combined role of bay and shelf modes in tsunami amplification along the coast*, J. Geophys. Res., *117*, C08027, doi:10.1029/2012JC008061.

BENAVENTE, R. and P. R. CUMMINS (2013), *Simple and reliable finite fault solutions for large earthquakes using the W-phase: The Maule (Mw= 8.8) and Tohoku (Mw= 9.0) earthquakes*, Geophys. Res. Lett., *40(14)*, 3591-3595.

BENAVENTE, R., P. R. CUMMINS and J. DETTMER (2016), *Rapid automated W-phase slip inversion for the Illapel great earthquake (2015, Mw = 8.3)*, Geophys. Res. Lett., *43*, doi:10.1002/2015GL067418.

BLASER, L., F. KRÜGER, M. OHRNBERGER and F. SCHERBAUM (2010), *Scaling relations of earthquake source parameter estimates with special focus on subduction environment*, Bull. Seismol. Soc. Am., *100*, 2914-2926.

CALISTO, I., M. ORTEGA and M. MILLER (2015), *Observed and modeled tsunami signals compared by using different rupture models of the April 1, 2014, Iquique earthquake*, Nat. Hazards, *79*, 397-408, doi:10.1007/s11069-015-1848-x.

COMPTE, D. and M. PARDO (1991), *Reappraisal of great historical earthquakes in the northern Chile and southern Peru seismic gaps*, Nat. Hazards, *4(1)*, 23-44, doi:10.1007/BF00126557.

DEMETS, C., R. G. GORDON, D. F. ARGUS and S. STEIN (1994), *Effect of recent revisions to the geomagnetic reversal time scale on estimates of current plate motions*, Geophys. Res. Lett., *21*, 2191-2194.

DZIEWONSKI, A. M., T.-A. CHOU and J. H. WOODHOUSE (1981), *Determination of earthquake source parameters from waveform data for studies of global and regional seismicity*, J. Geophys. Res., *86*, 2825-2852, doi:10.1029/JB086iB04p02825.

EKSTRÖM, G., M. NETTLES and A. M. DZIEWONSKI (2012), *The global CMT project 2004-2010: Centroid-moment tensors for 13,017 earthquakes*, Phys. Earth Planet. Inter., *200-201*, 1-9, doi:10.1016/j.pepi.2012.04.002.

HAYES, G. P., L. RIVERA and H. KANAMORI (2009), *Source Inversion of the W-Phase: Real-time Implementation and Extension to Low Magnitudes*, Seismol. Res. Lett., *80(5)*, 817-822, doi:10.1785/gssrl.80.5.817.

HAYES, G.P., D. J. WALD and R. L. JOHNSON (2012), *Slab1.0: a three-dimensional model of global subduction zone geometries*, J. Geophys. Res., *117*, 1-15.

HICKS, S. and A. RIETBROCK (2015), *Seismic slip on an upper-plate normal fault during a large subduction megathrust rupture*, Nature Geoscience, *8*, 955-960, doi:10.1038/ngeo2585.

KAMIGAICHI, O., *Tsunami forecasting and warning. Extreme environmental events complexity in forecasting and early warning (ed. Meyers R.A.)*, Springer, New York (2011), pp. 982-1007, doi:10.1007/978-1-4419-7695-6_52.

KANAMORI, H. and D. ANDERSON (1975), *Theoretical basis of some empirical relations in seismology*, Bull. Seismol. Soc. Am., *65(5)*, 1073-1095.

KANAMORI, H. (1993), *W Phase*, Geophys. Res. Lett., *20(16)*, 1691-1694.

KANAMORI, H. and L. RIVERA (2008), *Source inversion of W phase: speeding up seismic tsunami warning*, Geophys. J. Int., *175*, 222-238, doi:10.1111/j.1365-246X.2008.03887.x.

LIU, P. L-F., S-B. WOO and Y-S. CHO (1998), *Computer Programs for Tsunami Propagation and Inundation*, Cornell University.

LOMNITZ, C. (1971), *Grandes Terremotos y Tsunamis en Chile Durante el Periodo 1535-1955*, Geofisica panamericana, *1(1)*, 151-178.

MASAMURA, K., K. FUJIMA, C. GOTO, K. IIDA and T. SHIGEMURA (2000), *Theoretical solution of long wave considering the structure of bottom boundary layer and examinations on wave decay due to sea bottom friction*, Journal of Hydraulic, Coastal and Environmental Engineering, JSCE, *No663/II-53*, pp. 69-78.

METOIS, M., C. VIGNY, A. SCQUET, A. DELORME, S. MORVAN, I. ORTEGA and C-M. VALDERAS-BERMEJO (2014), *GPS-derived interseismic coupling on the subduction and seismic hazards in the Atacama region, Chile*, Geophys. J. Int., *196*, 644-655.

MORENO, M., M. ROSENAU and O. ONCKEN (2010), *2010 Maule earthquake slip correlates with pre-seismic locking of Andean subduction zone*, Nature, *467*, 198-202.

MUROTANI, S., K. SATAKE and Y. FUJII (2013), *Scaling relations of seismic moment, rupture area, average slip and asperity size for M 9 subducting-zone earthquakes*, Geophys. Res. Lett., *40*, 5070-5074.

OKADA, Y. (1985), *Surface deformation due to shear and tensile faults in a half-space*, Bull. Seismol. Soc. Am., *75*, 1135-1154.

PAPAZACHOS, B. C., E. SCORDILIS, D. PANAGIOTOPOULOS, C. PAPAZACHOS and G. KARAKAISIS (2004), *Global relations between seismic fault parameters and moment magnitude of earthquakes*, Bull. Geol. Soc. Of Greece, *36*, 1482-1489.

PARDO, M., D. COMPTE and T. MONFRET (2012), *Seismotectonic and stress distribution in the central Chile subduction zone*, J. South Am. Earth Sci., *15(1)*, 11-22.

SCHURR, B., G. ASCH, S. HAINZL, J. BEDFORD, A. HOECHNER, M. PALO, R. WANG, M. MORENO, M. BARTSCH, Y. ZHANG, O. ONCKEN, F. TILMANN, T. DAHM, P. VICTOR, S. BARRIENTOS and J-P. VILOTTE (2014), *Gradual unlocking of plate boundary controlled initiation of the 2014 Iquique earthquake*, Nature, *512*, 299-302, doi:10.1038/nature13681.

SPARKES, R., F. TILMANN, N. HOVIUS and J. HILLIER (2010), *Subducted seafloor relief stops rupture in South American great earthquakes: Implications for rupture behaviour in the 2010 Maule, Chile earthquake*, Earth Planet Sci. Lett., *298*, 89-94.

STERN, C. (2004), *Active Andean volcanism: its geologic and tectonic setting*, Rev. Geol. Chile, *31*, 161-206.

STRASSER, F. O., M. C. ARANGO and J. J. BOMMER (2010), *Scaling of the source dimensions of interface and intraslab subduction-zone earthquakes with moment magnitude*, Seismol. Res. Lett., *81*, 941-950.

TANG, L., V. V. TITOV, C. MOORE and Y. WEI (2016), *Real-Time Assessment of the 16 September 2015 Chile Tsunami and Implications for Near-Field Forecast*, Pure and Appl. Geophys., *173(2)*, 369-387, doi:10.1007/s00024-015-1226-3.

TASSARA, A., H. J. GOTZE, S. SCHMIDT and R. HACKNEY (2006), *Three-dimensional density model of the Nazca plate and the Andean continental margin*, J. Geophys. Res., *111(B9)*, doi:10.1029/2005JB003976.

TOLKOVA, E. (2010), *EOF analysis of a time series with application to tsunami detection*, Dyn. Atmos. Oceans, *50/1*, 35-54, doi:10.1016/j.dynatmoce.2009.09.001.

VIGNY, C., A. RUDLOFF, J-C. RUEGG, R. MADARIAGA, J. CAMPOS and M. ALVAREZ (2009), *Upper plate deformation measured by GPS in the Coquimbo Gap, Chile*, Phys. Earth planet. Inter., *175(1-2)*, 86-95.

WANG, X. (2009), *User Manual for COMCOT version 1.7 (first draft)*, Cornell University.

WESSEL, P., W. H. F. SMITH, R. SCHARROO, J. LUIS and F. WOBBE (2013), *Generic Mapping Tools: Improved Version Released*, EOS Trans. AGU, *94(45)*, 409-410.

YAMAZAKI, Y. and K. F. CHEUNG (2011), *Shelf resonance and impact of near-field tsunami generated by the 2010 Chile earthquake*, Geophys. Res. Lett., *38*, L12605, doi:10.1029/2011GL047508.

YE, L., T. LAY, H. KANAMORI and K. D. KOPER (2016), *Rapidly Estimated Seismic Source Parameters for the 16 September 2015 Illapel, Chile $M_W 8.3$ Earthquake*, Pure and Appl. Geophys., *173(2)*, 321-332, doi:10.1007/s00024-015-1202-y.